Fermilab FERMILAB-Conf-03/200-E July 2003

Measurement of the $t\bar{t}$ cross section at $\sqrt{s} = 1.96$ TeV

The DØ Collaboration

Preliminary Result Presented at Winter Conferences 2003

Abstract

A measurement of the $t\bar{t}$ cross section at $\sqrt{s} = 1.96$ TeV is carried out on data samples of $\approx$40 pb^{-1} in dilepton channels ($e\mu$, ee and $\mu\mu$) and lepton+jets channels using two complementary approaches: a fully topological analysis and a soft-muon-tag. Overall, 17 events are observed with an expected background of 6.5 ± 0.6. This excess corresponds to an observation probability of three standard deviations and the measured $t\bar{t}$ cross section is:

$$\sigma_{p\overline{p}\to t\bar{t}} = 8.5^{+4.5}_{-3.6}\ \text{(stat)}\ ^{+6.3}_{-3.5}\ \text{(sys)}\ \pm 0.8\ \text{(lumi)}\ \text{pb}.$$

1 Introduction

At the center of mass energy of 1.96 TeV, top quarks can be produced singly or in pairs. The two cross sections are of similar magnitude but the single top events are much more difficult to distinguish from background and their signal has yet to be observed. This paper is concerned only with $t\bar{t}$ pair production. In leading-order QCD (LO), $\mathcal{O}(\alpha_s^2)$, $t\bar{t}$ production proceeds mostly through the $q\bar{q} \to t\bar{t}$ channel contributing to $\approx$90% of the cross section, and the $gg \to t\bar{t}$ processes contributes at the $\approx$10% level. The most recent calculations of the $t\bar{t}$ cross section provide predictions for $\sigma_{p\overline{p}\to t\bar{t}}$ ranging from 5.4 to 7.4 pb [1].

In the Standard Model, the top quark is expected to decay predominantly into a W boson and a b quark. The channels in which the top quark is sought are determined therefore by the decay modes of the two W bosons. The channels can be classified as follows: the dilepton channel, where both W bosons decay leptonically into an electron or a muon (ee, $\mu\mu$, $e\mu$), the lepton + jets channel where one of the W bosons decays leptonically and the other hadronically (e+jets, μ+jets), and the all-jets channel where both W bosons decay hadronically. This note will focus entirely on the dilepton and lepton + jets channels. Tau decays are not considered because of the larger amounts of background they involve. For the lepton+jets channels two approaches are used: a topological analysis, using only kinematic selection criteria, and a soft-lepton tag (SLT, here only a soft-muon tag within a jet is considered), where at least one jet is required to be tagged as a b-jet from the presence of a non-isolated soft-muon.

2 Detector and Object Identification

2.1 The DØ detector

The mechanical features and geometry of the DØ calorimeter have not changed since Run I, but its readout electronics and trigger processor were rebuilt to cope with the faster bunch-crossing rate in Run II. The new DØ inner tracker has a 2 T field produced by a ≈ 1.2 m diameter solenoid. The tracker consists of a fiber detector (CFT) and of silicon detectors (SMT). The CFT is made of 830 μm diameter scintillating fibers, read out by cryogenic visible-light photon counters (VLPC), arranged in 8 layers within radii from 20 to 60 cm [2]. SMT [3] silicon modules (both single and double sided) are arranged in disks and polygons structures centered on the beam [3]. The luminosity monitor is made of two scintillator systems placed around the beam pipe at $\approx \pm 140$ cm of the nominal interaction point [4]. Scalers record correlated pairs of hits during the live time of the acquisition system to provide the exposed luminosity.

2.2 Electron Identification

Electrons are identified as EM clusters in the calorimeter associated with a nearby charged particle track. EM clusters are required to have a large fraction of energy in the EM section of the calorimeter $f_{\rm EM} \equiv E_{\rm EM}/E_{\rm tot} > 0.9$, where $E_{\rm EM}$ is the cluster energy in the EM section of the calorimeter within a cone of radius $\mathcal{R} \equiv \sqrt{\Delta\eta^2 + \Delta\varphi^2} = 0.2$ and $E_{\rm tot}$ is its total energy in the same cone. In addition, the energy deposition is compared to that of simulated electron showers by means of a χ^2, and accepted as a cluster when $\chi^2 < 20$. The sample is further restricted to isolated clusters by requiring that the total energy contained between a cone of radius $\mathcal{R} = 0.4$ and a cone of radius $\mathcal{R} = 0.2$ is less than 15% of the energy deposited within the inner cone of $\mathcal{R} = 2$. The energy of the candidate electrons are corrected for the non linearity of the readout chain and gain dispersion in individual channels and energy loss in material before the calorimeter. The absolute energy scale is set by requiring that the $Z \to e^+e^-$ peak lie at its known mass of 91.2 GeV.

2.3 Muon Identification

Muons are identified using the muon system and the central tracker. The muon signature in the calorimeter is used only to measure the identification efficiency. First, muons are identified in the muon system. Cosmic muons are removed by requiring that the time difference between hits in scintillator layers are consistent with a muon coming from the interaction region. The muon tracks are then extended to the point of closest approach (PCA) to the beam, and their parameters compared with tracks from the central tracking device [2, 3]. A global fit is performed to all central tracks that are matched in azimuthal and polar angles to a muon track. A muon is thus isolated when the energy deposited in the calorimeter in a cone between an inner radius of 0.1 and an outer radius of 0.4 is $< 2.5\ GeV$ and the scalar sum of the transverse momenta of all tracks within $R = 0.5$ of the jet does not exceed 2.5 GeV.

2.4 Jet Identification

Jets are reconstructed at DØ using the *improved legacy cone* algorithm, designed following the recommendation of the Run2 QCD workshop. Seed towers are composed of the sum of all cells that share the same pseudo-rapidity as estimated assuming particles are originating from the geometrical center of the detector (η_d) and azimuthal angle. A cone radius of R=0.5 is chosen for the following analyses. Jet quality criteria to remove rare jets which are clustered from fluctuations of noise in the calorimeter (particularly in its coarse hadronic section) are applied.

2.5 Jet Energy Scale

Because of the presence of regions with un-instrumented material, noise and shower fluctuations, the measured energy in a jet cone is not equal to the emitted parton energy. Jet energies are corrected using the relationship [5]:

$$E = \frac{E_{measured} - O}{R \times S}$$

where R is the fractional calorimeter response to jets obtained from balancing E_T in γ+jets events. O is the energy offset due to the underlying event, energy pile-up, multiple interactions, electronic noise, and uranium noise from the uranium absorber. O is determined from energy densities observed in minimum-bias events. S is the fraction of shower that leaks out of the R=0.5 jet cone in the calorimeter, as determined from observed energy profiles of jets. The same procedure is applied to data and Monte Carlo.

2.6 Missing Transverse Energy

The possible presence of a neutrino in the final state can be inferred from the imbalance in momentum in the transverse plane that it generates. The vector sum of any transverse energies in excess of 100 MeV in all layers of the calorimeter[1] yields a measure of this imbalance, and thereby provides an indirect estimate of the transverse momentum of the neutrino. The vector momentum opposite to this imbalance is often called the missing transverse-energy vector, and its value is termed the uncorrected (or observed) missing transverse energy ($\not\!\!E_T{}^{obs}$).

The response of the calorimeter to electromagnetic particles such as photons or electrons is different from that to hadrons. In events containing both electromagnetic objects and jets, this difference translates into an effective missing transverse energy. To correct this artificial imbalance, the appropriate part of the JES correction, *i.e.* the response R, applied to all good jets is subtracted from the uncorrected $\not\!\!E_T$, thereby providing a corrected calorimetric missing transverse energy ($\not\!\!E_T{}^{cal}$).

All matched muons in the event can be subtracted from the missing transverse energy vector, and their expected energy deposition in the calorimeter (≈ 2 GeV) can also be deducted to form a total $\not\!\!E_T{}^{tot}$ that takes account of all corrections.

[1]Except for those in the coarse hadronic layer, which are treated separately due to their high levels of noise. The only cells of the coarse hadronic calorimeter that are used in the sum are those clustered within good jets.

Table 1: Specific trigger requirements and integrated luminosities for each channel. The numbers before EM and JT indicate the number of EM or Jet objects required in the trigger, and the numbers in parentheses denote their E_T thresholds in GeV.

	Trigger Requirements			
Channel	Level 1	Level 2	Level 3	$\int \mathcal{L}dt$
e+jets	2JT(5) & 1EM(10)	2JT(10) & 1EM(10)	1EM(15) & 2JT(15)	49.5
μ+jets	1Muon & 1JT(5)	1Muon	1JT(20)	40.0
ee	2EM(10)	none	1EM(20)	48.2
$\mu\mu$	2Muons	1Muon	none	42.6
$e\mu$	1Muon & 1EM(5)	none	1EM(10)	33.0

3 Data Sets

The analyses reported herein are based on datasets taken from August 15, 2002, until January 12, 2003, where 96.8pb^{-1} were delivered to the experiment, 68.2 pb^{-1} were recorded and 66.5 pb^{-1} were reconstructed. As the various analysis channels have different trigger criteria and different quality requirements, the integrated luminosity corresponding to each channel is listed in Table 1.

3.1 Triggers, Data Quality and Luminosities

Specific triggers have been designed to cope with the high luminosity and to efficiently select $t\bar{t}$ events, for each analysis channel. At Levels 1 and 2 jets and electrons are triggered using 0.2×0.2 towers in the calorimeter and muons are triggered using the PDT and scintillator systems in the central region and the MDT in the forward region. At Level 3, the calorimeter information is read out providing better identification of electrons and jets, using criteria close to those used in offline reconstruction. The trigger selection criteria are summarized in Table 1.

To ensure uniform and reliable data, quality requirements are applied to the 66.5 pb^{-1} of reconstructed events. These requirements are based on the status of the calorimeter and the muon spectrometer hardware and on the reconstruction software. Channels involving muons have more stringent quality criteria than those involving only calorimetric objects, and therefore have less luminosity.

3.2 Monte Carlo Simulation

All signal and background processes are generated at $\sqrt{s} = 1.96$ TeV. The leading order CTEQ4L [6] parton distribution functions are used. $t\bar{t}$ events are simulated using PYTHIA 6.203 [7] at a top quark mass of 175 GeV. W+jets events are simulated using the leading-order VECBOS [8] matrix elements, coupled to HERWIG [9] to simulate the underlying event, initial state

radiation, parton hadronization, and the decay of the W boson. All other backgrounds are generated using PYTHIA. After hadronization, all signal and background events have additional minimum bias proton-antiproton events superposed. The number of added events is taken from a Poisson distribution with a mean of 0.5. The events are then processed through full GEANT simulation of the DØ detector.

4 Dilepton Analyses

The analysis of dilepton channels follows closely those carried out on Run I data, except in the treatment of muons where the additional information from the central tracking system provides far higher precision to the momentum measurement.

4.1 The $\mu\mu$ and ee Channels

The ee and $\mu\mu$ channels correspond to a small branching ratio of $t\bar{t}$ events (1/81 each). The signature for dileptonic decays of the top quark corresponds to two isolated leptons of high-p_T, two high-p_T b-quark jets, and a large $\not\!\!E_T$ from the two neutrinos. The dominating backgrounds for this signature are either from the mismeasurement of the $\not\!\!E_T$ or misidentification of jets. These include: $Z \to \ell^+\ell^-$, which has a large cross section but no significant $\not\!\!E_T$, heavy-flavor quark production with two objects misidentified as isolated leptons, and W+jets with one jet misidentified as an isolated lepton. Physically irreducible backgrounds, such as, $Z \to \tau\tau$ and $WW \to \ell^+\ell^-$, have very low rates.

Instrumental background for dilepton channels arises either from the effect of mismeasurements of energy in the calorimeter, which produces a non-negligible probability for an event without neutrinos to develop substantial $\not\!\!E_T$, or from non-isolated muons or electromagnetic jets that can appear isolated or EM-like and pass identification criteria. For both the dielectron and the dimuon channels, instrumental backgrounds are estimated using the probability that background events pass the $\not\!\!E_T$ selection, and that an electron or a muon in a background event is found and appears isolated. These probabilities are evaluated from background data samples.

The dimuon channel selection criteria require two isolated muons with $p_T > 15$ GeV, at least two jets with $p_T > 20$ GeV, $\not\!\!E_T > 25$ GeV, for $M_{\mu\mu} < 70$ GeV or $M_{\mu\mu} > 110$ GeV, $\not\!\!E_T > 40$ GeV, for 70 GeV $< M_{\mu\mu} < 110$ GeV, and $H_T > 100$ GeV, where H_T is the scalar sum of the jet transverse energies.

The dielectron channel selection criteria require two matched electrons with $p_T > 20$ GeV, at least two jets with $p_T > 20$ GeV, $\not\!\!E_T > 25$ GeV, for $M_{ee} < 75$ GeV or $M_{ee} > 105$ GeV, and $\not\!\!E_T > 40$ GeV, for 75 GeV $< M_{ee} < 105$ GeV, and $H_T^e > 120$ GeV, where H_T^e is the scalar sum of the transverse energies of jet and EM objects.

Altogether, 0.6 ± 0.3 ee and 1.0 ± 0.5 $\mu\mu$ background events are expected with ≈97% (and ≈98%) being due to instrumental backgrounds. Assuming a production cross section of 7 pb, 0.3 events are expected in each channel. Two events are observed in $\mu\mu$ data, and four events are collected in ee data.

The results for the ee and $\mu\mu$ channels are summarized in Table 2.

4.2 The $e\mu$ Channel

The $e\mu$ decay channel is the cleanest of the dilepton channels. The $e\mu$ background contributions fall into two general categories: instrumental backgrounds, arising from misidentification of objects, and irreducible backgrounds that contribute true prompt $e\mu$ events. The instrumental backgrounds are mainly from heavy flavor events, with a false electron and a misidentified isolated muon, or from W+jets, with a false electron or a misidentified isolated muon. The irreducible backgrounds are of similar nature as those in the dimuon channel, *i.e.*, $Z \to \tau\tau$ and $WW \to e\mu$. Instrumental backgrounds are estimated from large samples of events with low missing transverse energy. The instrumental background is constructed from a sample in which the electron requirements are loosened to the point that the electrons contribute negligibly in comparison to jets. This sample is then scaled by the rate at which jets mimic electrons. The selection criteria are $\not\!\!E_T > 10$ GeV, $\not\!\!E_T{}^{cal} > 20$ GeV, and at least two jets with $p_T > 20$ GeV. The scalar sum of the transverse energies of the jets and the EM cluster must also exceed 120 GeV.

Altogether, 0.1 ± 0.1 background events are expected ($\approx$70% from instrumental sources). Assuming a production cross section of 7 pb, 0.50 events are expected, and one event is observed. The results for the $e\mu$ channel are summarized in Table 2.

5 Lepton+Jets Analyses

The characteristic topology of the lepton+jets signature is one isolated high-E_T electron or muon, a large $\not\!\!E_T$ and four or more high-E_T jets. The two main backgrounds are from W+jets production and multijet events, containing a jet misidentified as an electron or an isolated muon, and mismeasured $\not\!\!E_T$. The analysis of these channels proceeds in two steps, which are conceptually similar for both the muon and electron channels. The first step consists of defining a data sample enriched in W+jets and top events, within which the absolute normalization of backgrounds from both W+jets and multijet production can be evaluated. In the second step, additional kinematic selections or soft-muon b-tagging criteria are applied to reach the final selection. In order to arrive at statistically independent samples, a soft-muon veto is applied to events used in the topological approach.

5.1 Topological Approach

5.1.1 The W+Jets Selections

A rather loose preselection of W and top events is used to evaluate the absolute normalization of both the W and multijet backgrounds. The e+jets analysis requires one EM particle with $E_T > 20$ GeV with $|\eta_d| < 1.1$ and, $\not\!\!E_T > 20$ GeV. The μ+jets analysis requires one reconstructed muon with $p_T > 20$ GeV, $\not\!\!E_T > 20$ GeV and, $\not\!\!E_T{}^{cal} > 15$ GeV.

5.1.2 Multijet Background

To obtain the number of W and $t\bar{t}$ events in the preselected sample, the contamination from multijet background is evaluated using two samples of events, one with loose restrictions and the other with greater restrictions, the latter being a subset of the first. For the e+jets (μ+jets) channel, the discrimination criterion is the match of the EM cluster to a central track (the muon isolation). The rates at which W and $t\bar{t}$ "signal" and multijet background events are filtered from one set to the other (respectively at efficiencies ε_{sig} and ε_{MJT}), are estimated respectively using control samples of Z production and low $\not\!\!E_T$ multijet data events. For all lepton+jets analyses we define the set of N^ℓ events as representing the loose preselection. For the e+jets analysis, direct-photon production and multijet events, where one jet is misidentified as an electron candidate, must be subtracted. The most restricted sample N^t is selected by requiring that the EM particle have a track match. For the μ+jets channel, the background is due primarily to heavy-flavour quark production, where the muon originates from a semi-leptonic heavy quark decay, and the more restricted muon sample is therefore defined with a selection on muon isolation. If the total number of "signal" and "background" events are denoted $N^{\mathrm{W+t\bar{t}}}$ and N^{MJT} respectively, N^ℓ and N^t can be written:

$$N^\ell = N^{\mathrm{W+t\bar{t}}} + N^{\mathrm{MJT}} \quad (1)$$

$$N^t = \varepsilon_{sig} N^{\mathrm{W+t\bar{t}}} + \varepsilon_{MJT} N^{\mathrm{MJT}} \quad (2)$$

Solving the equations for N^{MJT} and $N^{\mathrm{W+t\bar{t}}}$ yields:

$$N^{\mathrm{W+t\bar{t}}} = \frac{N^t - \varepsilon_{MJT} N^\ell}{\varepsilon_{sig} - \varepsilon_{MJT}} \quad \text{and} \quad N^{\mathrm{MJT}} = \frac{\varepsilon_{sig} N^\ell - N^t}{\varepsilon_{sig} - \varepsilon_{MJT}} \quad (3)$$

The transverse W mass distribution in each multiplicity bin is shown in Figs. 1 and 2, together with the contribution from multijet background, using the separation in Eq. 3, which will be referred to as the matrix method.

5.1.3 Berends Scaling

To extract the top signal from the overwhelming multijet and W+jets background, at least four jets are required to be reconstructed. In the case of the e+jets analysis, jets are accepted only when clustered at pseudo-rapidities within $|\eta| < 2.0$, whereas in the μ+jets analysis jets are required to be within $|\eta| < 2.5$. In both cases, only jets with transverse energy in excess of 15 GeV are considered. The $t\bar{t}$ contribution is deduced from a separate estimate of the W+jets background. The latter is evaluated assuming Berends' empirical scaling law, which relates cross sections for the n^{th} and the $(n+1)^{th}$ jet multiplicities as follows [10]:

$$\frac{\sigma[W + (n+1)\ jets]}{\sigma[W + n\ jets]} = \alpha$$

where α depends on jet transverse energy and pseudo-rapidity, and n is the inclusive jet multiplicity. After subtraction of multijet background using the Matrix Method, the number of W+jets events with jet multiplicity $\geq i$ is given by:

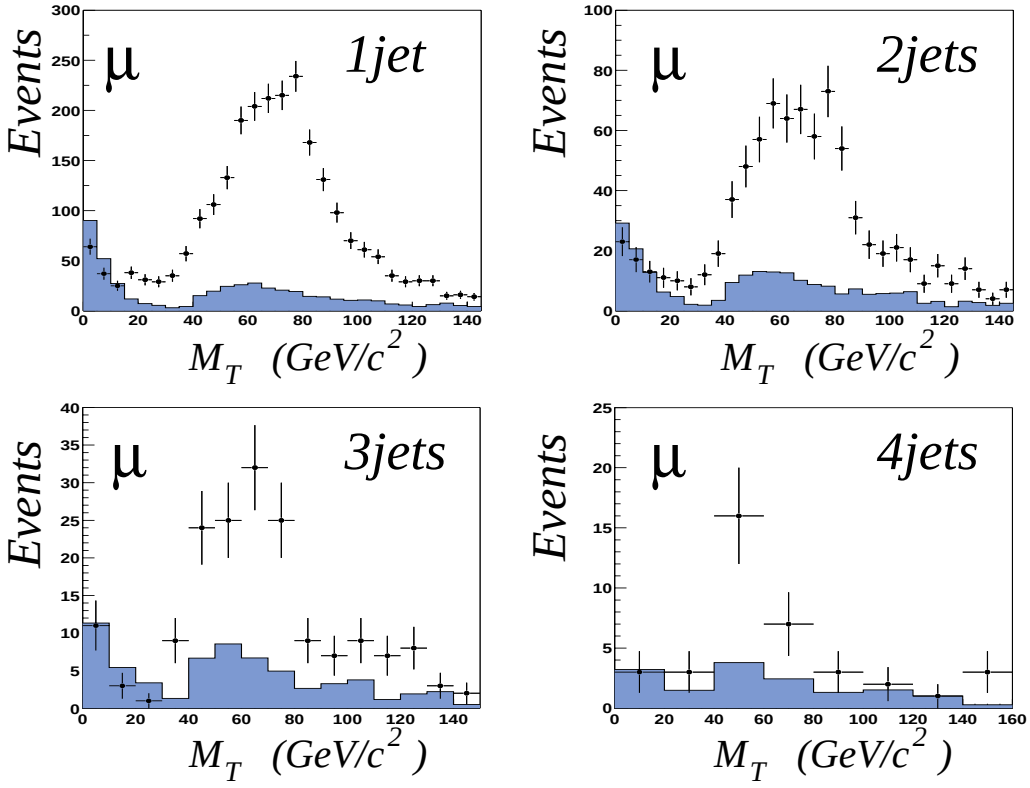

Figure 1: Transverse mass distribution on the ≥ 1, ≥ 2, ≥ 3, and ≥ 4-jet multiplicity bins. Dots are the observed numbers of events after selections, histograms represent the multijet background contribution. The two-peak structure observed in the "background" distribution results from kinematic requirements and two distinct topological configurations: (1) the muon is pointing in the direction of the missing transverse energy and (2) it is pointing opposite of the missing transverse energy.

$$N_i^{\mathrm{W+t\bar{t}}} = N_1^W \times \alpha^{i-1} + f_i^{t\bar{t}} N_i^{t\bar{t}}$$

where $N_i^{\mathrm{W+t\bar{t}}}$ is the number of events once the multijet background is subtracted, N_1^W is the number of W events with at least one jet in the final state, as estimated by the Matrix Method, $f_i^{t\bar{t}}$ is the fraction of $t\bar{t}$ events expected to be present in the more restricted sample with a jet multiplicity $\geq i$. This fraction is computed from a Monte Carlo simulation. In the topological analyses, the values of α, N_1^W, and $N_i^{t\bar{t}}$ can be obtained from a fit to the distribution of $N^{\mathrm{W+t\bar{t}}}$ for $i = 1, 2, 3, 4$. We only use the α parameter to extrapolate the number of W events in the ≥ 4 jets topology:

$$N_4^W = N_1^W \times \alpha^3$$

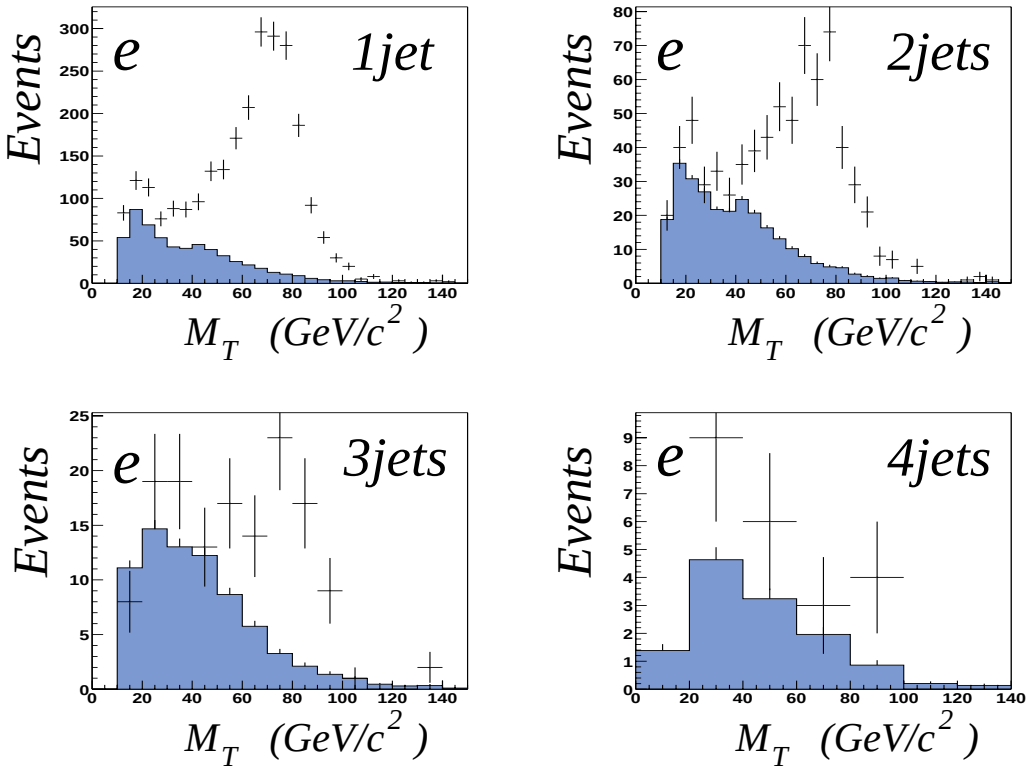

Figure 2: Transverse mass distribution on the ≥ 1, ≥ 2, ≥ 3, and ≥ 4-jet multiplicity bins. Dots are the observed numbers of events after selections, histograms represent the multijet background contribution. The two-peak structure observed in the "background" distribution results from kinematic requirements and two distinct topological configurations: (1) the electron is pointing in the direction of the missing transverse energy and (2) it is pointing opposite of the missing transverse energy.

The original suggestion of Berends scaling is based on the character of the ISR gluon spectrum in W events [10]. However, the inclusive jet-multiplicity distribution for W and $t\bar{t}$ events is highly biased by jet selection criteria of the trigger. A correction factor for each inclusive jet multiplicity is therefore derived from unbiased data samples triggered with single electron and single muon requirements for use in the e+jets and μ+jets analyses, respectively. The extrapolated number of W events in the fourth bin corresponds to an estimate without trigger bias. To measure the number of W+4-jets events selected by the trigger ($\tilde{N}_4^W$) the trigger efficiency (ε_{4j}^W) is evaluated from a Monte Carlo simulation, and applied to the data:

$$\tilde{N}_4^W = \varepsilon_{4j}^W N_4^W$$

The two most discriminating variables used in RunI [11] to attain best separation between signal and background in the lepton+jets analyses were the scalar sum over all jet transverse

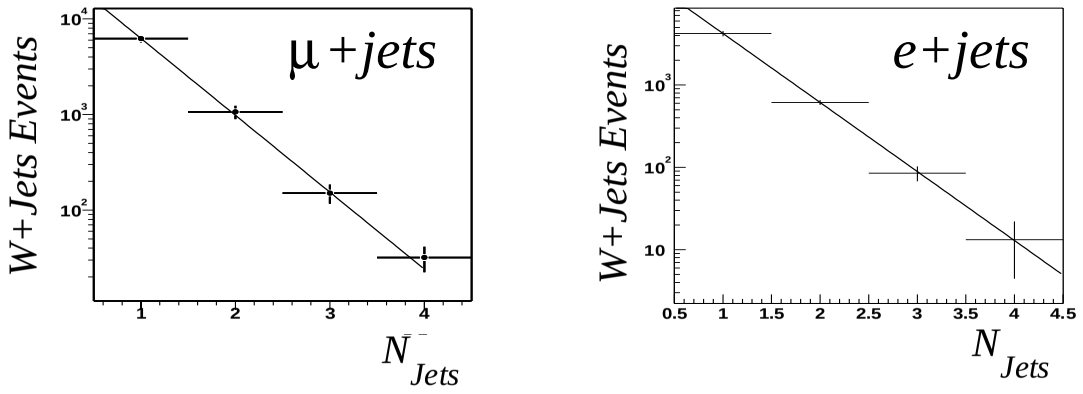

Figure 3: Yield of inclusive W+N_jets as a function of N_{jets}, for the μ+jets and e+jets analyses.

energies $H_T = \Sigma_{jets} E_T$ and the aplanarity $\mathcal{A}$, a measure of the planarity of an event [11]. Large values of $\mathcal{A}$ are indicative of spherical events. For the case of the e+jets (μ+jets), selections were made at $\mathcal{A} > 0.065$ and $H_T > 180$ GeV ($\mathcal{A} > 0.0065$ and $H_T > 220$ GeV)[2].

After applying the topological selections from Run I, four events were observed in both the e+jets and μ+jets channels, while 2.7 ± 0.6 and 2.7 ± 1.1 were expected from background processes, respectively. For a $t\bar{t}$ cross section of 7 pb, 1.8 ± 0.4 and 2.4 ± 0.4 signal events were expected. The results for these channels are summarized in Table 2.

5.2 Soft Muon b Jet Tagging

The analyses of the lepton+jets channels with soft-muon tags use exactly the same preselections as the topological analysis, except that the veto on soft muons is removed and that the requirement on $\not\!\!E_T{}^{cal}$ in the μ+jets channel is not imposed. In the following, only jets with $E_T > 20\,\text{GeV}$ and $|\eta_d| < 2$ are considered, unless otherwise specified. A milder selection is first applied, requiring at least three jets, $\mathcal{A} > 0.04$, and $H_T > 110$ GeV. There are 23 and 22 events surviving in the electron and muon channels, respectively.

Soft-muon tagging is applied to these selected events. A jet is termed tagged if a muon with $p_T > 4\,\text{GeV}/c$ and $|\eta| < 2$ is found within $\Delta R = 0.5$ of the jet axis. This leaves two events in the e+jets channel, both in the four-jet topology, and none in the μ+jets channel.

The multijet background in the final samples is again evaluated using the Matrix Method. The less restricted electron sample contains nine events, and the analogous muon sample contains one event. The signal and background efficiencies for moving events from the less to the more restricted samples are identical to those determined in the topological analyses as a function of the jet multiplicity. The multijet background evaluated in this way amounts to

[2]For the μ+jets analysis, the H_T variable is defined to contain the transverse momentum of the leptonic W, which is the vector sum of the p_T of the muon and the $\not\!\!E_T$.

$N_{MJT} = 0.20 \pm 0.09$ and 0.23 ± 0.23 in the e+Jets and μ+jets channels, respectively.

The background from W+jets is obtained by applying a tagging probability to the samples of 23 e+jets and 22 μ+jets untagged events, after subtraction of multijet background as performed in the tagged samples. There are 459 (64) untagged events with a loosely identified electron (loosely isolated muon), and hence 9.6 ± 1.3 (13.1 ± 2.4) untagged W+jets events in the electron (muon) + jets channels.

The jet-tagging probability (or "tag-rate") was determined as a function of jet p_T, η and φ, using a sample of multijet events containing at least four jets. The heavy-flavor content of such multijet events is believed to be similar to that of W+jets events. A systematic uncertainty of 20% is ascribed to the tag rate function to cover the uncertainty of this assumption; this evaluation relies on studies of the heavy-flavor content of W+jets events as a function of the jet multiplicity, performed with the ALPGEN generator [12]. The average event tag rate for the untagged W+jets events is 0.016, in the e+jets and μ+jets channels, leading to expected numbers of tagged events from this source of $N_{W+jets} = 0.15 \pm 0.04$ and 0.21 ± 0.06, respectively. However, these estimates include the contributions from the untagged top events, calculated as if the tag rate for such events were the same as that for multijet events. The tagging probability for top events, as determined from Monte Carlo, is 0.15, which is sufficiently different from the tag rate for untagged events to allow the W+jets and top contributions to be disentangled. The numbers of top events in the final samples are obtained from the formula

$$N_{top} = N_{data} - N_{MJT} - (N_{W+jets} - k_{top} N_{top})$$

with $k_{top} = 0.016/0.15$. The total backgrounds in the e+jets and μ+jets channels are 0.16 ± 0.10 and 0.74 ± 0.38, respectively. Altogether, two events are observed in the lepton+jets channels, over a total background of 0.90 ± 0.39.

The numbers of top events expected to be selected and tagged are estimated from Monte Carlo to be 1.4 in the combined e+jets and μ+jets channels, assuming an effective integrated luminosity of $40\,\mathrm{pb}^{-1}$, obtained by requiring that both the muon system and the calorimeter function properly, and a production cross section of 7 pb. The overall selection efficiencies are 1.3% and 2.0% in the e+jets and μ+jets channels, respectively. The results for these two channels are also summarized in Table 2.

6 Systematic uncertainties

Systematic uncertainties can be separated into five categories: uncorrelated background, uncorrelated signal, correlated background, correlated signal, and uncertainties in luminosity.

The uncorrelated uncertainties in background are typically from limitations in data or statistics of the Monte Carlo. For instance, the uncertainty on the estimate of the number of multijet events in the 4^{th} bin in lepton+jets analyses, is partially obtained by using a background sample different from that used in the evaluation of the signal, and partially from the Matrix Method. The latter makes use of signal efficiency and is thereby correlated with signal. As the overall uncertainty on the background estimate is not dominated by this contribution, this correlation is neglected. For lepton+jets analyses, the uncertainty on the

Table 2: Summary of individual analysis channel.

	Dilepton Channels						
	N^{obs}	Signal	$\mathcal{B}$	Bkg.	$\int \mathcal{L}dt$	ε	σ (pb)
ee	4	0.25	0.012	1.00	48.2 pb^{-1}	5.9%	$105.9^{+82.1}_{-59.6}(stat)^{+96.2}_{-39.7}(sys)$
$\mu\mu$	2	0.28	0.012	0.59	42.6 pb^{-1}	7.7%	$35.8^{+42.9}_{-28.0}(stat)^{+24.4}_{-11.5}(sys)$
$e\mu$	1	0.50	0.025	0.07	33 pb^{-1}	8.9%	$13.2^{+19.3}_{-10.1}(stat)^{+4.7}_{-0.8}(sys)$
	Lepton-plus-jets Channels (topological)						
	N^{obs}	Signal	$\mathcal{B}$	Bkg.	$\int \mathcal{L}dt$	ε	σ (pb)
e+jets	4	1.8	0.147	2.7	49.5 pb^{-1}	3.5%	$5.2^{+9.4}_{-6.7}(stat)^{+9.1}_{-3.1}(sys)$
μ+jets	4	2.4	0.147	2.7	40.0 pb^{-1}	5.8%	$3.8^{+6.9}_{-4.9}(stat)^{+3.9}_{-5.4}(sys)$
	Lepton-plus-jets Channels (Soft Muon b Tag)						
	N^{obs}	Signal	$\mathcal{B}$	Bkg.	$\int \mathcal{L}dt$	ε	σ (pb)
e+jets	2	0.5	0.147	0.16	40.0 pb^{-1}	1.3%	$24.1^{+23.0}_{-14.3}(stat)^{+7.0}_{-4.6}(sys)$
μ+jets	0	0.8	0.147	0.74	40.0 pb^{-1}	2.0%	$< 8.5(stat)$

estimate of the number of W's in the 4^{th} bin comes from the correlated propagation of the uncertainties on α and N_1^W in the fit to Berends' scaling. The uncertainty on the background evaluation for the muon channel is larger than that for the electron channel. This is mostly due to the larger uncertainty on the trigger bias, given the weaker statistics of the unbiased single-muon trigger, which was prescaled more than the single electron trigger. The part of the uncertainty in the uncorrelated background contribution arising from Monte Carlo statistics in the evaluation of background efficiencies for topological variables is negligible. The uncorrelated signal uncertainties are essentially those due to the Monte Carlo statistics.

Most of the systematic uncertainties in signal are correlated with the background. The uncertainty on the p_T of the muon comes from comparing the effect of nominal smearing in the Monte Carlo (smearing added to simulate data distributions) and no smearing. The uncertainty on μ-ID is derived from the absolute error on the muon ID efficiency. The uncertainty on jet resolution is derived assuming a jet energy resolution worse by 20%. The uncertainty in jet energy scale is derived by varying the nominal jet correction by $\pm 1\sigma$; this contributes to both signal efficiency and background. The uncertainty on the Jet ID is derived from the variation in Jet Id efficiency obtained from samples of dijet events and γ+jets events, in data and in Monte Carlo. The error on the luminosity is assumed to be 10%. Systematic uncertainties neglect any correlation between signal and background arising from to the fact that most backgrounds are evaluated from data. A summary of the systematic uncertainties and their inter-channel correlation is given in Table 3. Using these values, the measured cross sections for individual channels are displayed in Table 2.

Table 3: Summary of systematic uncertainties, where Δb is the basolute uncertainty on the background and $\Delta\varepsilon$ is the relative uncertainty on the efficiency in %.

		ee		$\mu\mu$		$e\mu$		μj		ej		μj/μ		ej/μ	
		Δb	$\Delta\varepsilon$	Δb	$\Delta\varepsilon$	Δb	$\Delta\varepsilon$	Δb	$\Delta\varepsilon$	Δb	$\Delta\varepsilon$	Δb	$\Delta\varepsilon$	Δb	$\Delta\varepsilon$
Uncorr.	All	0.48	10	0.3	3.8	0.04	0.4	1.1	1.4	0.6	3.6	0.3	1.4	0.10	3.6
Correlated e	e_{trk}	-	6.1	-	-	-	3.1	-	-	-	3.1	-	-	-	3.1
	e_{ID}	-	4.9	-	-	-	2.5	-	-	-	2.5	-	-	-	2.5
Correlated μ	p_T^μ	-	-	-	2	-	0.8	-	0.8	-	-	-	0.8	-	-
	μ_{ID}	-	-	-	10	-	3	-	3	-	-	-	3	-	-
Correlated Jet	JES	-	3.7	-	3.7	-	3.7	-	$^{+3.9}_{-13.1}$	-	$^{+15.1}_{-19.7}$	-	$^{+3.9}_{-13.1}$	-	$^{+15.1}_{-19.7}$
	Jet $_{ID}$	-	4	-	4	-	4	-	8	-	8	-	8	-	8
	Jet res.	-	4	-	4	-	4	-	2.8	-	2.8	-	2.8	-	2.8

7 Conclusion

A first measurement of the $t\bar{t}$ cross section at the new Tevatron center-of-mass energy of 1.96 GeV was performed in two dilepton channels ($e\mu$ and $\mu\mu$) and four lepton+jets channels (e+jets, μ+jets, e+jets/μ and μ+jets/μ). The individual results of each analysis are summarized in Table 2 and in Figure 4. The expected number of signal events displayed therein are obtained assuming a $t\bar{t}$ cross section of 7 pb.

The combined result yields a measured cross section of:

$$\sigma_{p\overline{p}\to t\bar{t}} = 8.5^{+4.5}_{-3.6}\ \text{(stat)}\ ^{+6.3}_{-3.5}\ \text{(sys)}\ \pm 0.8\ \text{(lumi)}\ \text{pb}.$$

Taking the systematic uncertainties on the background estimate into account, the significance of the observation corresponds to a three-standard-deviations effect.

References

[1] M. Cacciari, S. Frixione, M. L. Mangano, P. Nason and G. Ridolfi, HEP-PH/0303085.

[2] A. Bross *et al.*, "The D0 scintillating fiber tracker," *Prepared for SCIFI97: Conference on Scintillating and Fiber Detectors, South Bend, Indiana, 2-6 Nov 1997.*

[3] B. Quinn [D0 Collaboration], "The D0 Silicon Microstrip Tracker," Nucl. Instrum. Meth. A **501** (2003) 7.

[4] C. C. Miao [D0 Collaboration], "The D0 Run II luminosity monitor," Nucl. Phys. Proc. Suppl. **78** (1999) 342.

[5] B. Abbott *et al.* [D0 Collaboration], "Determination of the absolute jet energy scale in the D0 calorimeters," Nucl. Instrum. Meth. A **424**, 352 (1999)

[6] H. L. Lai *et al.*, "Global QCD analysis and the CTEQ parton distributions," Phys. Rev. D **51**, 4763 (1995)

[7] T. Sjostrand, L. Lonnblad and S. Mrenna, "PYTHIA 6.2: Physics and manual," hep-ph/0108264.
T. Sjostrand, "High-energy physics event generation with PYTHIA 5.7 and JETSET 7.4," Comput. Phys. Commun. **82**, 74 (1994).

[8] F. A. Berends, H. Kuijf, B. Tausk and W. T. Giele, "On The Production Of A W And Jets At Hadron Colliders," Nucl. Phys. B **357**, 32 (1991).

[9] G. Marchesini, B. R. Webber, G. Abbiendi, I. G. Knowles, M. H. Seymour and L. Stanco, "HERWIG: A Monte Carlo event generator for simulating hadron emission reactions with interfering gluons. Version 5.1 - April 1991," Comput. Phys. Commun. **67**, 465 (1992).
G. Corcella *et al.*, "HERWIG 6: An event generator for hadron emission reactions with interfering gluons (including supersymmetric processes)," JHEP **0101**, 010 (2001)

[10] F. A. Berends, J. B. Tausk and W. T. Giele, "Top search in multi - jet signals," Phys. Rev. D **47**, 2746 (1993).

[11] V. M. Abazov *et al.* [D0 Collaboration], Phys. Rev. D **67**, 012004 (2003)

[12] M. L. Mangano, M. Moretti, F. Piccinini, R. Pittau and A. D. Polosa, "ALPGEN, a generator for hard multiparton processes in hadronic collisions," hep-ph/0206293.

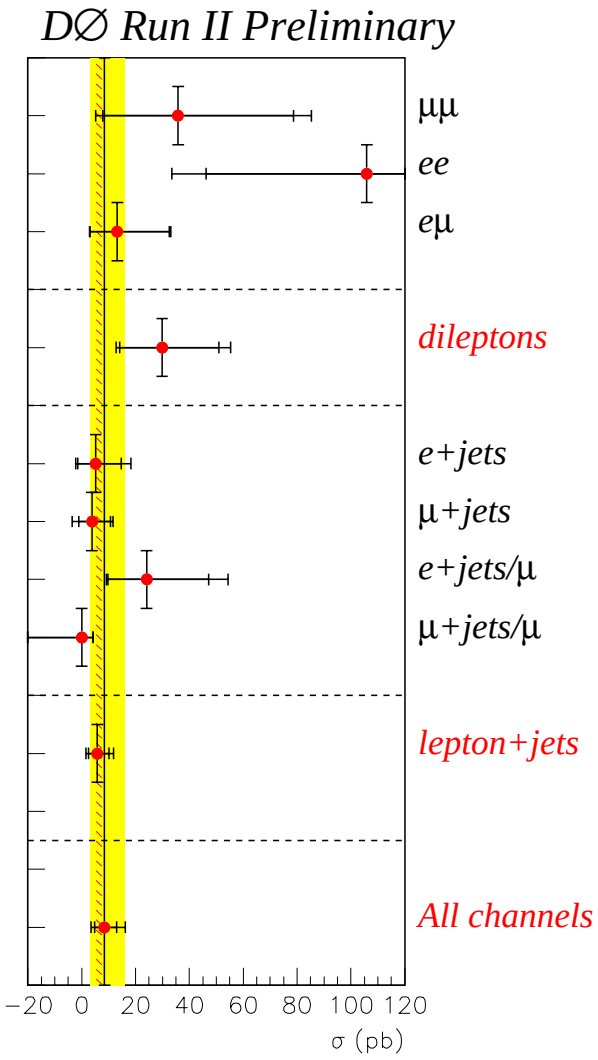

Figure 4: Summary of individual cross sections, dilepton and lepton+jets subcombinations, and the full combination of measurements. The theoretical prediction is indicated by the slanted band.